NASA/TP-1998-207643

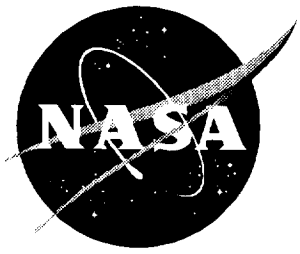

Development of In-Fiber Reflective Bragg Gratings as Shear Stress Monitors in Aerodynamic Facilities

Devendra S. Parmar
Hampton University, Hampton, Virginia

Danny R. Sprinkle and Jag J. Singh
Langley Research Center, Hampton, Virginia

National Aeronautics and
Space Administration

Langley Research Center
Hampton, Virginia 23681-2199

April 1998

Available from the following:

NASA Center for AeroSpace Information (CASI)
7121 Standard Drive
Hanover, MD 21076-1320
(301) 621-0390

National Technical Information Service (NTIS)
5285 Port Royal Road
Springfield, VA 22161-2171
(703) 487-4650

Abstract

Bragg gratings centered at nominal wavelengths of 1290 nm and 1300 nm were inscribed in a 9/125 μm germano-silicate optical fiber, using continuous wave frequency doubled Ar^+ laser radiation at 244 nm. Such gratings have been used extensively as temperature and strain monitors in smart structures. They have, however, never been used for measuring aerodynamic shear stresses. As a test of their sensitivity as shear stress monitors, a Bragg fiber attached to a metal plate was subjected to laminar flows in a glass pipe. An easily measurable large flow-induced wavelength shift ($\Delta\lambda_B$) was observed in the Bragg reflected wavelength. Thereafter, the grating was calibrated by making one time, simultaneous measurements of $\Delta\lambda_B$ and the coefficient of skin friction (C_f) with a skin friction balance, as a function of flow rates in a subsonic wind tunnel. Onset of fan-induced transition in the tunnel flow provided a unique flow rate for correlating $\Delta\lambda_B$ and C_f values needed for computing effective modulus of rigidity (η_{eff}) of the fiber attached to the metal plate. This value of η_{eff} is expected to remain constant throughout the elastic stress range expected during the Bragg grating aerodynamic tests. It has been used for calculating the value of C_f at various tunnel speeds, on the basis of measured values of Bragg wavelength shifts at those speeds.

Introduction

Fiber gratings are excellent transducer elements, since they are integral to the light-guiding fiber core and are highly wavelength selective. The extremely narrow bandwidth of the reflected light makes them particularly sensitive sensors for temperature (ref. 1) and strain (ref. 2). The temperature sensitivity arises largely from the effect on the refractive index of the fiber, rather than from the change in the grating constant. The strain, however, affects both the grating constant and the refractive index (ref. 3). Fiber gratings have never been used for shear stress measurements—mainly because the silica fibers are very hard and it is very difficult to separate the strain effects from the shear stress effects. It does, however, appear that the shear stress effects can be separated from the strain effects under properly designed experimental conditions. These shear stress effects, though small, would be measurable with currently available narrow line width commercial Bragg gratings.

The hardness of the glass fiber can work to the experimenter's advantage, since the shear angle will be so small that it will not affect the transmissibility of the reflected signal along the core. We have measured shear stress effects on fiber gratings in the laboratory as well as in a wind tunnel. The results of our studies are described in this publication.

Symbols

a, b	constants
C_f	coefficient of skin friction
$d\lambda_B/dT$	temperature coefficient of Bragg wavelength
I	intensity measure at wavelength
L	grating constant
n	refractive index of fiber
S	shearing stress
T	temperature
V	velocity
η_{eff}	effective modulus of rigidity
λ_B	Bragg wavelength
λ_{BO}	reflected Bragg wavelength in absence of shear stress
λ_{BS}	shear-induced Bragg wavelength

λ_{BT} temperature-induced Bragg wavelength

λ_0 position of peak centroid

ρ air density

σ half-width

ϕ shear strain

Theoretical Background

The wavelength of the Bragg reflected wave is related to the grating constant L and the refractive index of the fiber n by the Bragg reflection condition, that is

$$\lambda_{BO} = 2nL \tag{1}$$

where λ_{BO} is the Bragg wavelength at room temperature in the absence of any shear stress.

As the fiber is subjected to a shearing stress S, the Bragg planes will be sheared through a small angle ϕ, with a concomitant small rise in temperature ΔT. Figure 1 illustrates the schematic diagram of a shear-stressed grating mounted on a flat plate.

The change in the Bragg wavelength ($\Delta\lambda_B$) is given by

$$\Delta\lambda_B = \Delta\lambda_{BT} + \Delta\lambda_{BS} \tag{2}$$

where

$\Delta\lambda_{BT}$ temperature-induced shift in Bragg wavelength

$\Delta\lambda_{BS}$ shear-induced shift in Bragg wavelength

Equation (2) assumes that the thermal and shear effects are essentially independent, a behavior which has been found to be valid for small perturbations (ref. 4).

It is not possible to separate the temperature and shear effects on the basis of a single wavelength shift in one grating. (It is, however, possible to make simultaneous measurements of temperature and shear stress if two Bragg gratings at wavelengths separated by several hundred nanometers are colocated and are simultaneously interrogated and subjected to the same aerodynamic [shear stress] forces.) However, the temperature coefficient ($d\lambda_B/dT$) can be determined by exposing the Bragg fiber to different temperatures without any shear force; $\Delta\lambda_{BT}$ is given by

$$\Delta\lambda_{BT} = \left(\frac{d\lambda_B}{dT}\right)\Delta T \tag{3}$$

This temperature-induced effect can be subtracted from the observed Bragg shift, leaving only the shear-induced effect.

The shear-induced wavelength shift ($\Delta\lambda_{BS}$) can also be described as follows:

$$\Delta\lambda_{BS} = 2nL\left[\frac{\Delta L}{L}\left(1+\frac{\Delta n}{n}\right)+\frac{\Delta n}{n}\right]$$

$$\approx 2nL\left(\frac{\Delta L}{L}\right)$$

(since $\Delta n/n << \Delta L/L << 1$) [1]

$$\Delta\lambda_{BS} = 2nL\left(\frac{L - L\cos\phi}{L}\right)$$

$$\Delta\lambda_{BS} \approx \lambda_{BO}\left(\frac{\phi^2}{2}\right) \tag{4}$$

Thus a measurement of Bragg wavelength change under an external shear stress S provides a direct measure of the shear strain ϕ induced by it. In our studies, the shear stress S was produced by allowing a stream of air having velocity V flow over a grating fiber attached to a flat metal plate, that is

$$S = C_f\left(\frac{1}{2}\rho V^2\right) \tag{5}$$

where C_f is the coefficient of skin friction and ρ is the air density.

[1]The wavelength shift in a fiber exposed to an orthogonal shear flow, after allowing for the temperature effect, was observed to be nearly zero (fig. 8), whereas there was an easily measurable shift in parallel flows. This lack of shift in the orthogonal grating indicates that $\Delta n/n << 1$ is not necessarily inconsistent with the earlier comment regarding the strain effect mentioned in the Introduction.

The effective modulus of rigidity (η_{eff}) of the grating fiber attached to the flat plate is given by

$$\eta_{eff} = \frac{S}{\phi} = C_f \frac{\rho V^2}{\left(8\frac{\Delta\lambda_{BS}}{\lambda_{BO}}\right)^{1/2}} \quad (6)$$

Clearly, the accuracy of η_{eff} depends strongly on the accuracy with which we can measure $\Delta\lambda_{BS}$. This will depend to a large extent on the Bragg grating bandwidth and the stability of the optical analyzer. We used a Hewlett Packard spectrum analyzer (model HP70951A) for measuring the Bragg spectrum. This is a diffraction grating-based optical spectrum analyzer that provides spectral measurements of optical power as a function of wavelength. Its nominal resolution for the 800–1700 nm range is 0.1 nm. However, by using the following procedures, we were able to measure wavelengths up to the third decimal place, that is 0.001 nm:

(1) First, the approximate position of the peak centroid (λ_0) was obtained by averaging the wavelengths of the data points at –6 dB on each side of the nominal peak position.

(2) This approximate centroid position value was then plugged in the following normal distribution expression for the least-squares fit of the data up to 20 channels on each side of the centroid position:

$$I(\lambda) = a_0 e^{-(\lambda-\lambda_0)^2/2\sigma_0^2} \quad (7)$$

The least-squares fit provided the values of a_0, λ_0, and σ_0 needed for the Bragg peak profile. In the present case, the bandwidth at 1300 nm was 0.4 nm at room temperature. The resolution of the entire wavelength analysis system, including the effects of the stability and repeatability of associated electronics, was determined to be of the order of 0.001 nm. The stability and repeatability of the Bragg analysis system are evidenced by the experimental measurements of λ_{BO}, after repeated thermal excursions, summarized in table 1.

Once η_{eff} has been determined for a particular fiber-plate assembly, it can be used to measure C_f for all other flow rates in the test chamber.

Experimental Procedure and Results

Two Bragg gratings centered at 1289.565 nm and 1299.432 nm at room temperature (25°C) were cowritten in the core of a 9/125 μm telecommunication fiber, doped with 10 weight percent germanium. These wavelengths were selected because they are near enough for interrogation by the same diode laser and yet separated enough to provide two simultaneous, independent measurements of $\Delta\lambda_B$. Since $\Delta\lambda_B/\lambda_B$ is expected to remain constant under a given shear stress, simultaneous measurements of $\Delta\lambda_B$ at two neighboring wavelengths should provide a reliable means for verifying the repeatability of our measurements.

The fiber was placed on a flat metal plate mounted inside a constant temperature enclosure. A thermocouple was also placed inside the constant temperature enclosure in the vicinity of the fiber. Figure 2 shows a schematic diagram of the experimental setup for the measurement of temperature dependence of the Bragg wavelengths.

The enclosure temperature was varied from the boiling point of liquid nitrogen (–196°C) to the boiling point of water (100°C) and Bragg wavelengths measured at a series of temperatures in that range. The results for the two gratings in the temperature range of 0°C to 35°C are shown in figures 3(a) and (b). It should be noted that $(d\lambda_B/\lambda_B)(1/dT)$ is 6.34 ± 0.03 ppm/1°C, in general agreement with the reported value for these fibers (ref. 5).

The fiber was next mounted in a 126-μm-deep groove, with a 127-μm-diameter semicircular bottom, etched in a flat metal plate used as the test model. A 1-μm-thick epoxy layer bonded the fiber to the metal plate. The top side of the bonded fiber was nearly flush with the metal plate surface. A thermocouple was also attached to the metal plate in the vicinity of the grating fiber.

Figure 4 shows the experimental details of the Bragg fiber mounted in the groove. The flat plate was mounted inside the constant temperature enclosure

and its temperature varied from −196°C to 100°C. A series of Bragg wavelength measurements were made in that range. The results for the temperature range of 0°C to 35°C are shown in figure 5. It is noted that $(d\lambda_B/\lambda_B)(1/dT)$ = 29.38 ± 1.00 ppm/1°C, about 4.6 times higher than the value measured for the free fiber. This difference is due to the mismatch in the coefficients of thermal expansion of the fiber and the epoxy. The thermal coefficients of expansion of the glass fiber and the epoxy are 1.3×10^{-5}/1°C and 6.0×10^{-5}/1°C, respectively (ref. 6). This mismatch is discussed in the section "Discussion."

The glued fiber-metal plate assembly, along with the thermocouple, was next mounted in the test section of a subsonic wind tunnel. A skin friction balance was mounted on the wall of the test section. Figure 6 shows the experimental setup used for $\Delta\lambda_B$ measurements inside the subsonic wind tunnel.

As the wind speed in the tunnel was increased from 0 to 90 m/sec, the Bragg reflected wavelengths and the fiber temperatures were monitored continuously. These results are summarized in table 2 and illustrated in figure 7(a). As a further check on the shear sensitivity of the Bragg fiber, we have compared the Bragg-derived temperatures with the thermocouple measurements.

Figure 7(b) shows the results when the observed $\Delta\lambda_B$ in a wind tunnel test is attributed solely to the temperature change. It is clear that the computed temperature is always lower than the thermocouple temperature. The difference is more marked for the laminar flow regime than for the turbulent regime because of flow disturbance (i.e., no or low shear stress) in the turbulent flow.

When the observed $\Delta\lambda_B$ in a thermally controlled enclosure is indeed solely due to the temperature change, the Bragg temperatures are in excellent agreement with the thermocouple measurements as illustrated in figure 7(c). These results clearly show that the values of $\Delta\lambda_B$ observed in wind tunnel tests are not entirely due to the temperature changes. Shear effects must be included to explain the Bragg wavelength changes.

It was noted that the Bragg wavelength, after allowing for the effects of the temperature change, decreased steadily until a wind speed of about 87 mph (38.89 m/sec) was reached, when it suddenly reversed trend with increasing speed. At the same speed, a sound pressure meter in the tunnel control room recorded a sudden increase in the sound pressure level, possibly indicating the onset of fan-induced flow transition in the tunnel flow. Also, at about the same wind speed, a similar change was noted in the output of the skin friction balance mounted on the tunnel wall. Near-simultaneous occurrence of these three independent events suggests that the Bragg reversal is related to the tunnel flow transition (from laminar to turbulent) at the Bragg fiber surface.

The critical speed at which the Bragg reversal occurs provides a very convenient calibration point for the "as-mounted" Bragg monitor. If we further assume that the C_f measured with the skin friction balance (ref. 7) mounted on the tunnel wall is the same as that on the fiber surface, equation (6) provides a direct measure of η_{eff} at the critical speed. This value can then be used to calculate C_f at any other tunnel speed.

Figure 8 shows Bragg wavelength changes in the two superimposed gratings as a function of the tunnel flow rate. The temperature effects have been subtracted from the observed wavelength changes. Also shown in this figure are the wavelength changes in a 1300 nm grating glued on the model and mounted orthogonal to the tunnel flow.[2] Clearly, there is no measurable change in the reflected Bragg wavelength in this grating, suggesting $\Delta n/n << 1$. (See footnote 1.) It also shows that the model deformation-induced strain in the Bragg fiber is negligible or immeasurable.

Figure 9(a) shows the skin friction balance output as a function of the air flow rate in the tunnel. Figure 9(b) shows Bragg wavelength change in the 1300 nm grating as a function of the tunnel flow rate. It should be noted that the Bragg grating is essentially a point measurement device, while the skin friction balance averages the C_f values over an area of an 8-in-diameter circular plate. This explains the difference in the sensitivity of the two devices noted in

[2]This grating was inscribed in our laboratory and had slightly different Bragg peak half-width and reflectivity compared with the parallel gratings. However, neither of these factors is expected to affect the results.

figure 9. However, both devices clearly show the onset of turbulence in the tunnel flow at a speed of 87 mph (38.89 m/sec).

Bragg data illustrated in figures 8 and 9(b) show an easily measurable change in Bragg wavelengths as a function of air flow along the fibers. Figures 9(a) and (b) clearly show a flow transition at 38.89 m/sec. This information was used to correlate Bragg wavelength changes with the coefficients of skin friction at various flow rates. For example, C_f at 38.89 m/sec is 0.0011. (See fig. 9(a).) Thus, with equation (6), η_{eff} can be calculated and, thereafter, C_f values at various tunnel speeds. The results are summarized in figure 10. The Blasius curve is also plotted in this figure. The Bragg-based skin friction data are in generally good agreement with the Blasius curve in the laminar flow regime.

Discussion

The experimental results discussed above indicate that the Bragg gratings can provide some very useful aerodynamic data. Since the temperature and shear stress effects are essentially uncoupled under typical wind tunnel testing conditions, the temperature effects on the Bragg data can be corrected for by either simultaneous temperature measurements or by using data from the orthogonally mounted grating. From data summarized in figures 8 and 9, the effective modulus of rigidity (η_{eff}) of the fiber-model assembly is calculated to be 6.8×10^7 N/m^2. This value is over 2 orders of magnitude lower than the value reported for silica fibers (ref. 6). It may be recalled that the grating is attached to the flat metal plate by means of a thin layer of epoxy glue. The thermodynamic properties of the epoxy are quite different from those of the silica fiber (ref. 6). This mismatch between the thermodynamic properties of the epoxy and the fiber may result in extra internal stresses in the fiber during the aerodynamic measurements. This argument is partially supported by the observations that the temperature effect on the Bragg wavelength in the case of glued fiber is considerably higher than in the case of free fiber (29.38 ± 1.00 ppm/1°C versus 6.34 ± 0.03 ppm/1°C). It would thus appear that the thin layer of epoxy bonding the grating fiber on the test surface enhances the shear-induced effect on the Bragg wavelength considerably.

Concluding Remarks

The Bragg wavelength changes track the skin friction values under similar wind tunnel flow conditions. The direction of Bragg wavelength change reverses when the flow character changes from the laminar to turbulent. The skin friction balance output also reverses trend at the same flow rate. By associating the skin friction value at the flow transition point with the Bragg wavelength change at that point, the Bragg sensor was calibrated for direct skin friction measurements at various tunnel speeds.

The temperature can be measured independently, and its effects allowed for by either a comounted thermocouple or another Bragg fiber mounted orthogonally to the fluid flow direction. It is also possible to make simultaneous measurements of temperature and shear stress during an aerodynamic test, if two colocated Bragg wavelengths differing by several hundred nanometers are simultaneously interrogated. It has been further noted that the epoxy adhesive used to bond the fiber on the test flat plate enhances the sensitivity of the Bragg shear monitor considerably.

NASA Langley Research Center
Hampton, VA 23681-2199
March 30, 1998

References

1. Kersey, Alan D.; and Dakin, John P.: *Distributed and Multiplexed Fiber Optic Sensors*. SPIE-1586, 1992, pp. 216–249.

2. Kersey, A. D.; Berkoff, T. A.; and Morey, W. W.: High-Resolution Fibre-Grating Based Strain Sensor With Interferometric Wavelength-Shift Detection. *Electron. Lett.*, vol. 28, Jan. 1992, pp. 236–238.

3. Morey, William W.; Ball, Gary A.; and Meltz, Gerald: Photoinduced Bragg Gratings in Optical Fibers. *Optics & Photo. News*, vol. 5, no. 2, Feb. 1994, pp. 8–14.

4. Xu, M. G.; Archambault, J.-L.; Reekie, L.; and Dakin, J. P.: Thermally-Compensated Bending Gauge Using Surface-Mounted Fibre Gratings. Int. J. Optoelectron., vol. 9, no. 3, 1994, p. 281.

5. Bennion, I.; Williams, J. A. R.; Zhang, L.; Sugden, K.; and Doran, N. J.: UV-Written In-Fibre Bragg Gratings. *Optical & Quant. Electron.*, vol. 28, no. 2, Feb. 1996, pp. 93–136.

6. Lynch, Charles T., ed.: *CRC Handbook of Materials Science*. CRC Press, 1980.

7. Winter, K. G.: *An Outline of the Techniques Available for the Measurement of Skin Friction in Turbulent Boundary Layers*. TM-AERO-1656, Royal Aircr. Establ., 1975.

Table 1. Summary of Bragg Wavelengths After Repeated Thermal Cycles

Date	Time	Temperature, °C	Bragg wavelength, nm
10/15/97	11:12 a.m.	25.9	1289.587
	01:10 p.m.	25.9	1289.587
	02:50 p.m.	25.9	1289.587
	03:30 p.m.	59.7	1290.997
	03.58 p.m.	59.7	1290.997
	04:18 p.m.	63.0	1291.113
	04:55 p.m.	63.0	1291.113
10/16/97	09:10 a.m.	25.9	1289.587
	11:15 a.m.	25.9	1289.587
	02:10 p.m.	25.9	1289.587

Table 2. Summary of Temperature and Bragg Wavelength Changes as Function of Tunnel Speed

Tunnel flow rate, mph	Bragg wavelength, λ_B, nm	Model temperature, T, °C	Temperature-induced Bragg wavelength changes, $\Delta\lambda_{BT}$, nm $\approx (d\lambda_B/dT)\Delta T$	Shear stress-induced Bragg wavelength changes, $\Delta\lambda_{BS}$, nm $\approx (d\lambda_B/dS)\Delta S$
0	1289.441	21.8	0.000	0.000
38.9	1289.410	21.0	–0.031	0.000
53.5	1289.408	21.0	–0.031	–0.002
61.6	1289.395	20.7	–0.043	–0.003
73.0	1289.397	20.8	–0.039	–0.005
80.3	1289.388	20.6	–0.047	–0.006
87.8	1289.378	20.4	–0.055	–0.008
94.7	1289.381	20.4	–0.055	–0.005
101.3	1289.403	20.9	–0.035	–0.003
116.9	1289.424	21.4	–0.016	–0.001
125.5	1289.440	21.8	0.000	–0.001
135.8	1289.452	22.1	0.012	–0.001
143.8	1289.463	22.4	0.023	–0.001
153.0	1289.475	22.7	0.035	–0.001
162.3	1289.483	22.9	0.043	–0.001
169.4	1289.495	23.2	0.055	–0.001
178.3	1289.502	23.4	0.062	–0.001
184.4	1289.506	23.6	0.070	–0.001
188.5	1289.503	23.5	0.066	–0.001
195.8	1289.521	23.9	0.082	–0.002

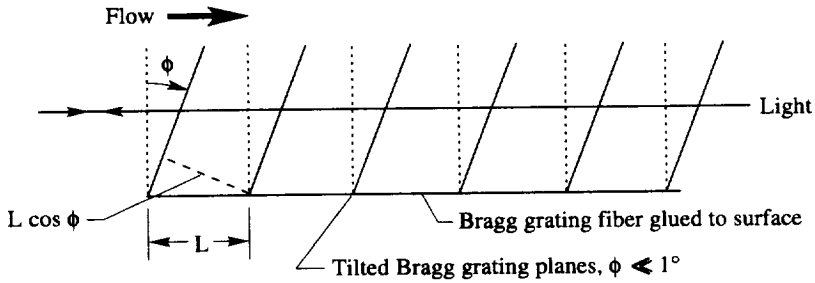

Figure 1. Schematic diagram of shear stressed grating mounted on flat plate.

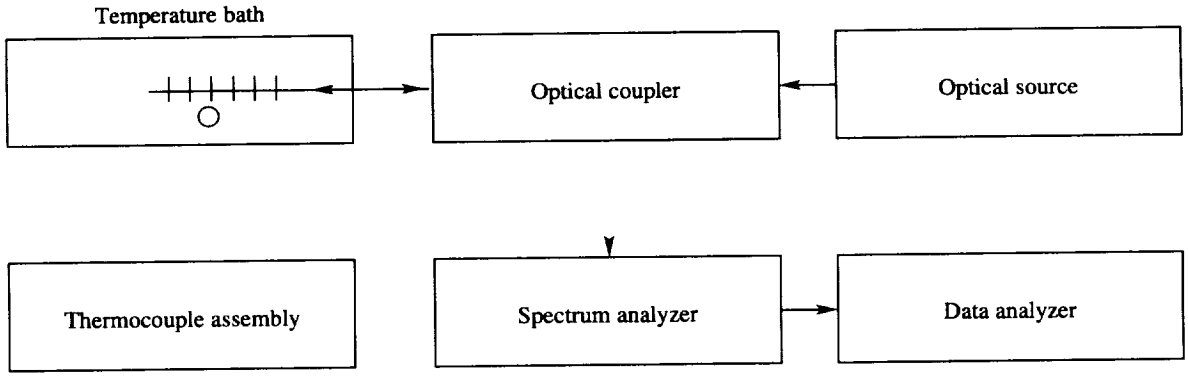

Figure 2. Schematic diagram of experimental setup for measurement of temperature dependence of Bragg wavelength.

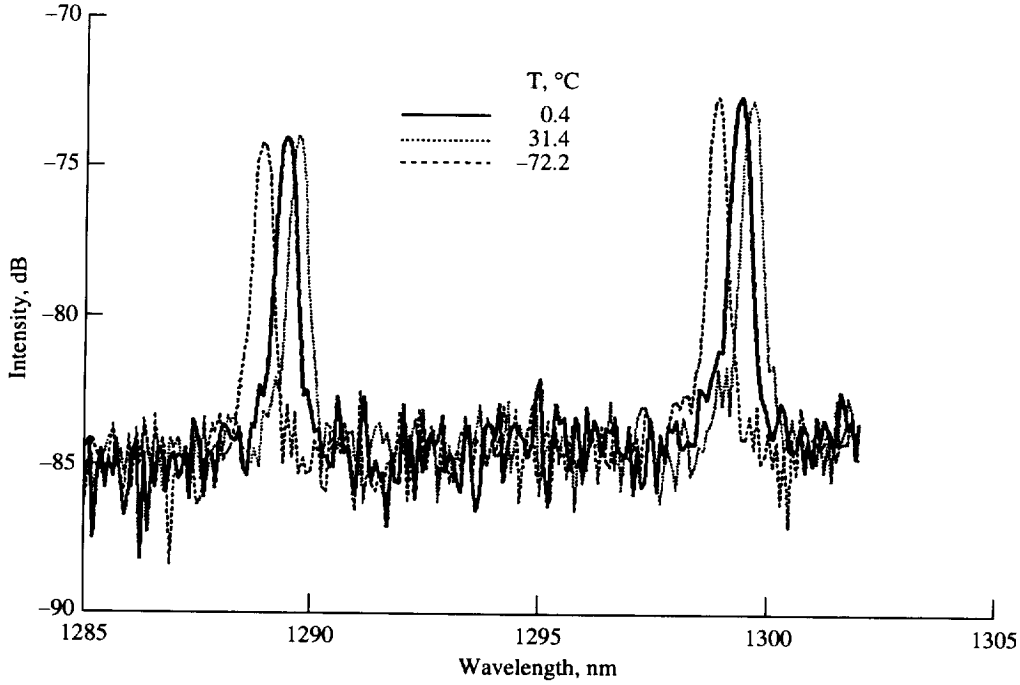

(a) Typical spectrum of double Bragg grating at three temperatures.

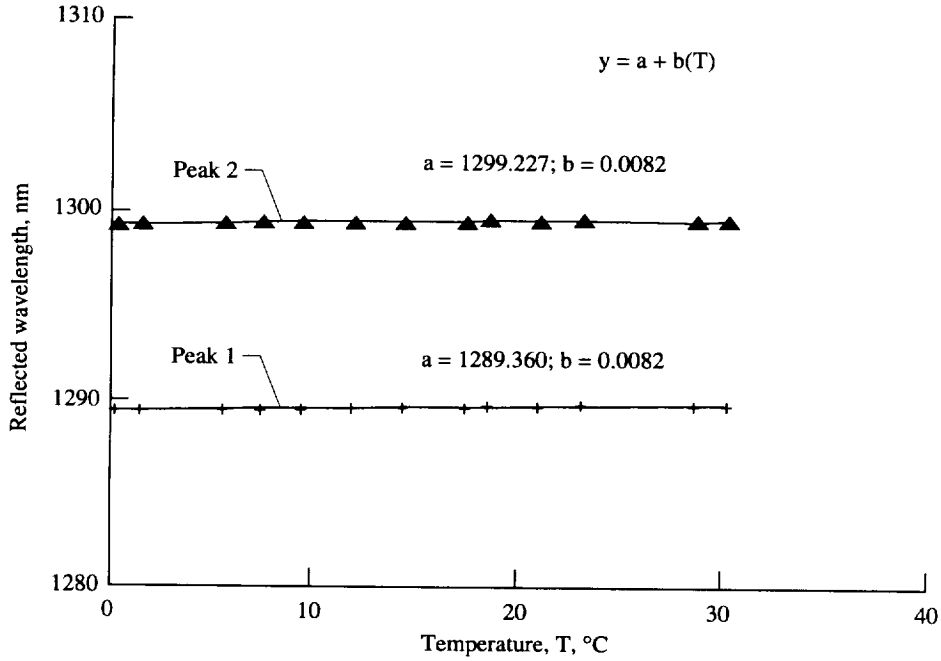

(b) Summary of temperature dependence of Bragg wavelength in free gratings.

Figure 3. Temperature dependence of Bragg wavelengths in free gratings.

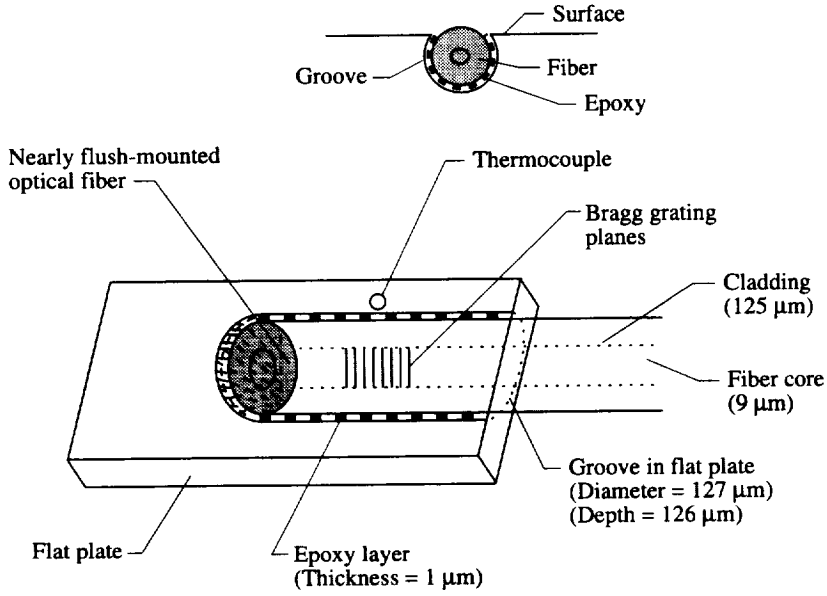

Figure 4. Details of Bragg fiber mounting on test model.

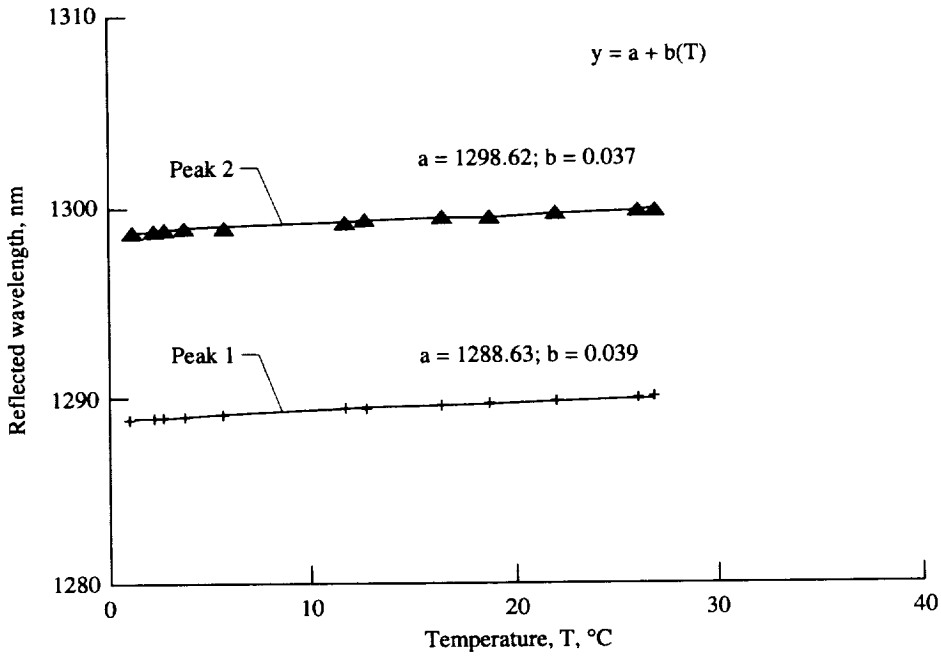

Figure 5. Temperature dependence of Bragg wavelengths in glued gratings.

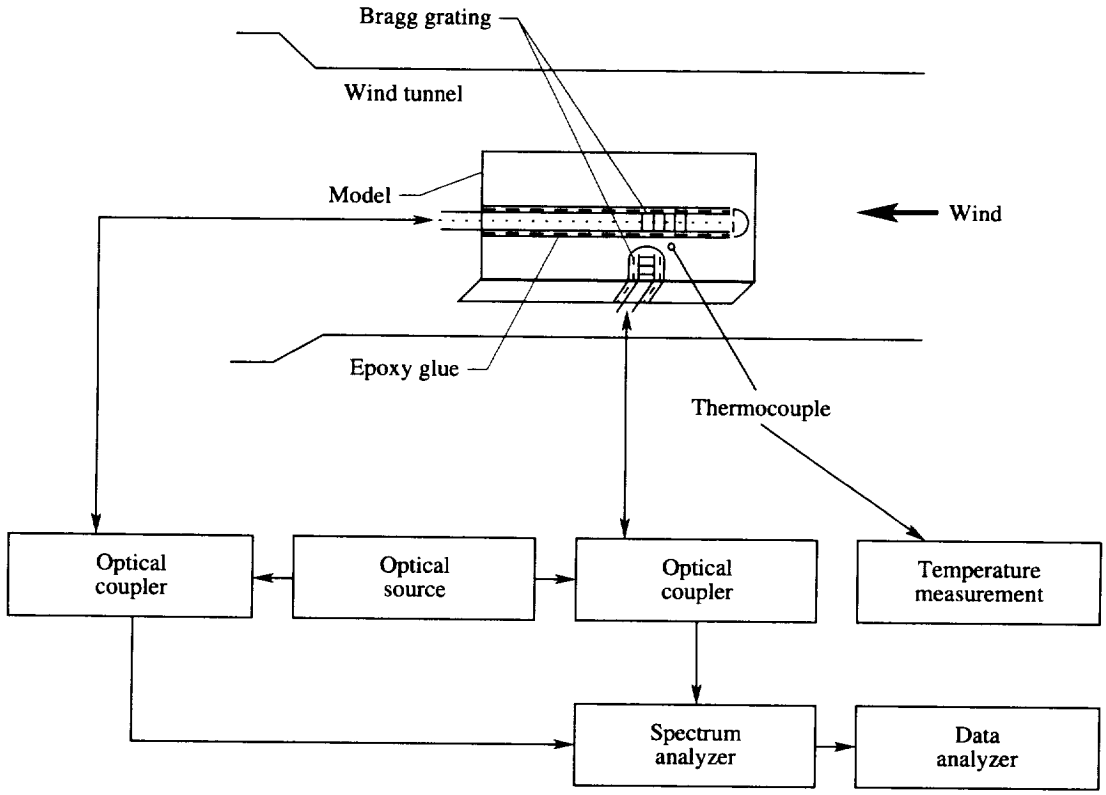

Figure 6. Schematic diagram of experimental setup for Bragg measurements inside subsonic wind tunnel.

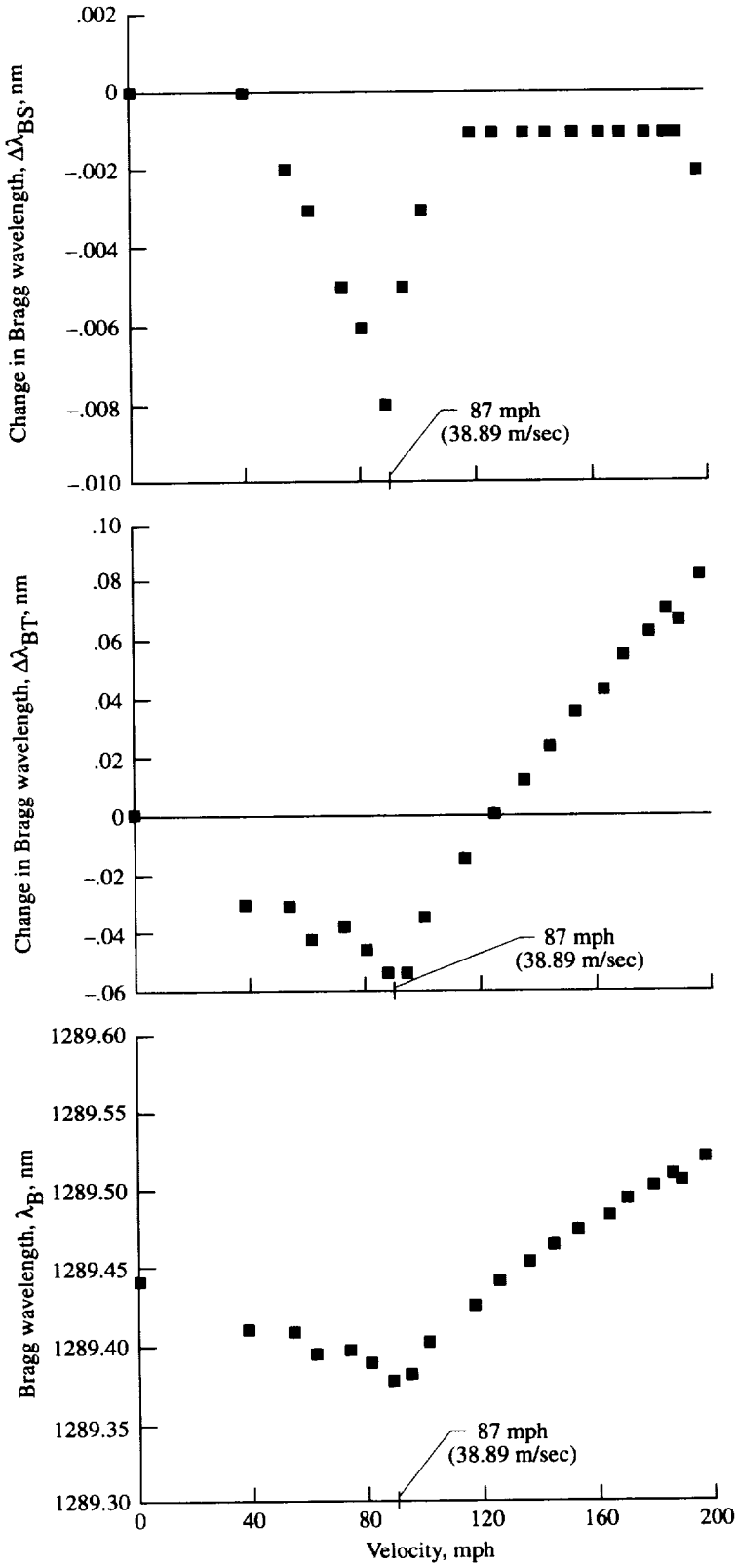

(a) Bragg wavelength changes as function of wind tunnel speed.

Figure 7. Temperature and Bragg wavelength changes in grating mounted on model as function of wind tunnel speed.

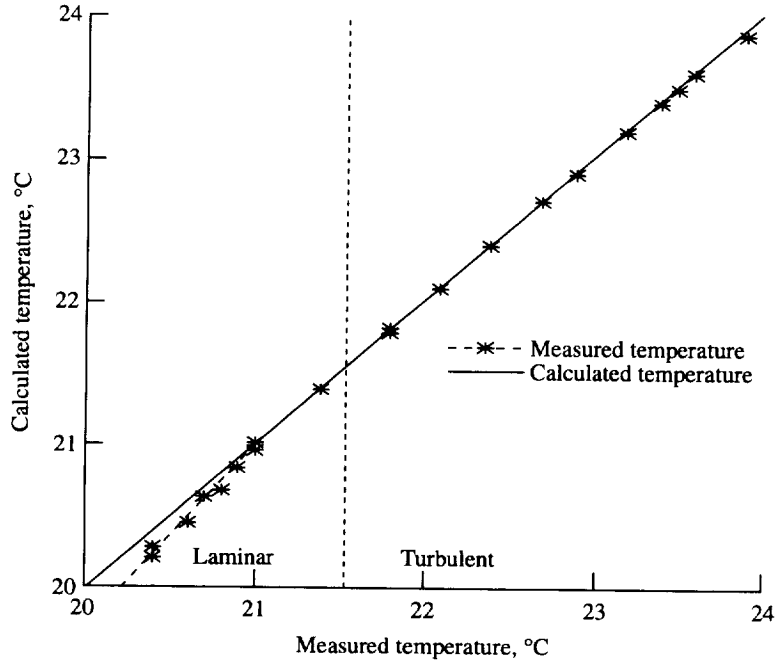

(b) Comparison between measured and calculated temperatures.

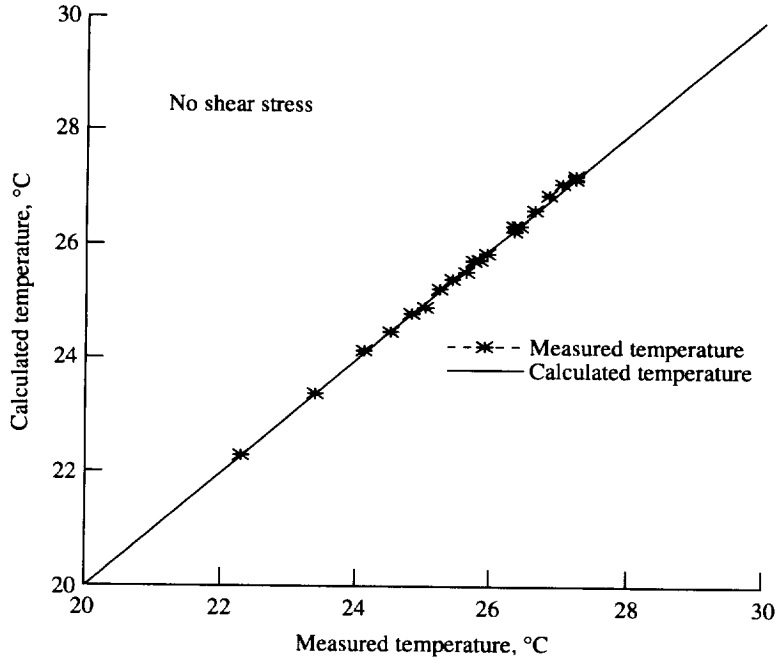

(c) Comparison between thermocouple temperature and temperature calculated from Bragg measurements.

Figure 7. Concluded.

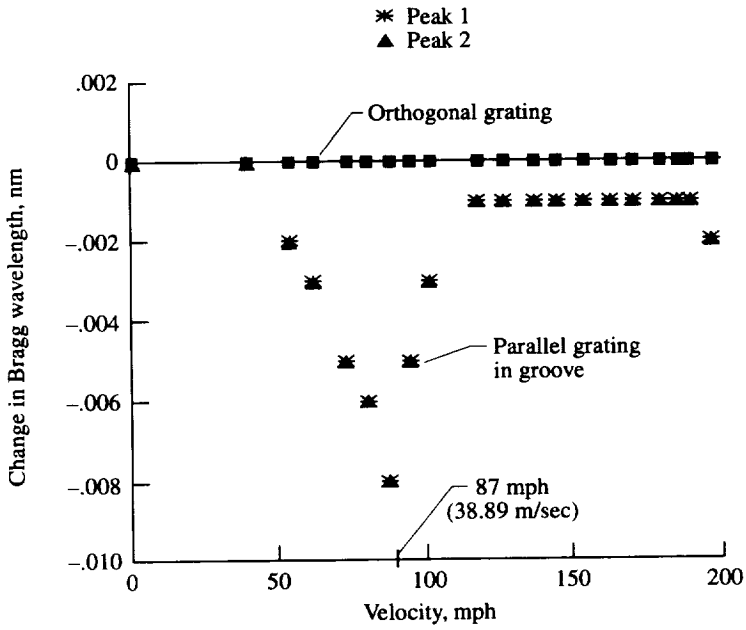

Figure 8. Bragg wavelength changes as function of tunnel speed.

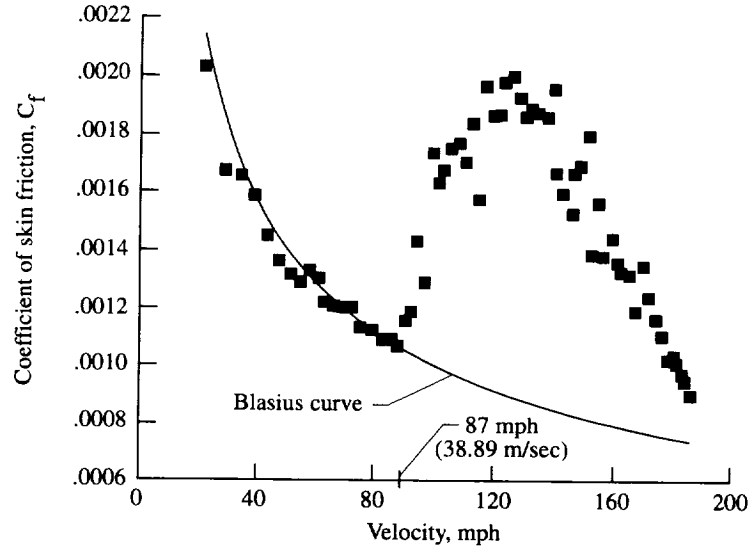

(a) Coefficient of skin friction versus tunnel speed as measured with skin friction balance mounted on wall.

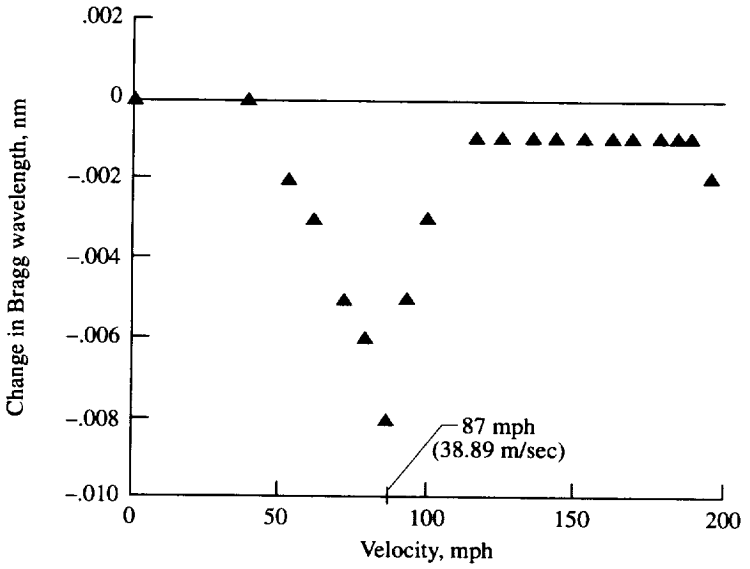

(b) Shear-stress-induced Bragg wavelength changes as function of tunnel speed.

Figure 9. Change in coefficient of skin friction as function of tunnel speed.

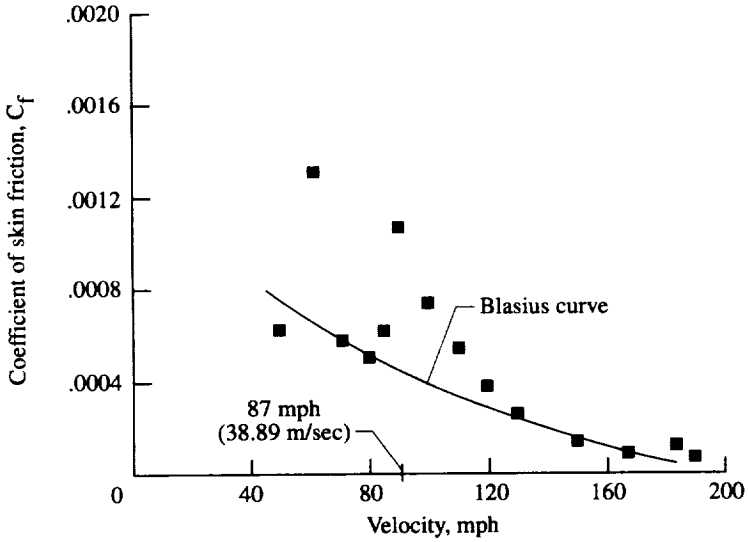

Figure 10. Coefficient of skin friction versus tunnel speed.

REPORT DOCUMENTATION PAGE

Form Approved
OMB No. 07704-0188

1. AGENCY USE ONLY *(Leave blank)*	2. REPORT DATE	3. REPORT TYPE AND DATES COVERED
	April 1998	Technical Publication

4. TITLE AND SUBTITLE
Development of In-Fiber Reflective Bragg Gratings as Shear Stress Monitors in Aerodynamic Facilities

5. FUNDING NUMBERS
WU 274-00-97-03

6. AUTHOR(S)
Devendra S. Parmar, Danny R. Sprinkle, and Jag J. Singh

7. PERFORMING ORGANIZATION NAME(S) AND ADDRESS(ES)
NASA Langley Research Center
Hampton, VA 23681-2199

8. PERFORMING ORGANIZATION REPORT NUMBER
L-17669

9. SPONSORING/MONITORING AGENCY NAME(S) AND ADDRESS(ES)
National Aeronautics and Space Administration
Washington, DC 20546-0001

10. SPONSORING/MONITORING AGENCY REPORT NUMBER
NASA/TP-1998-207643

11. SUPPLEMENTARY NOTES
Parmar: Hampton University, Hampton, VA; Sprinkle and Singh: Langley Research Center, Hampton, VA.

12a. DISTRIBUTION/AVAILABILITY STATEMENT
Unclassified–Unlimited
Subject Category 35 Distribution: Standard
Availability: NASA CASI (301) 621-0390

12b. DISTRIBUTION CODE

13. ABSTRACT ***(Maximum 200 words)***
Bragg gratings centered at nominal wavelengths of 1290 nm and 1300 nm were inscribed in a 9/125 μm germano-silicate optical fiber, using continuous wave frequency doubled Ar^+ laser radiation at 244 nm. Such gratings have been used extensively as temperature and strain monitors in smart structures. They have, however, never been used for measuring aerodynamic shear stresses. As a test of their sensitivity as shear stress monitors, a Bragg fiber attached to a metal plate was subjected to laminar flows in a glass pipe. An easily measurable large flow-induced wavelength shift ($\Delta\lambda_B$) was observed in the Bragg reflected wavelength. Thereafter, the grating was calibrated by making one time, simultaneous measurements of $\Delta\lambda_B$ and the coefficient of skin friction (C_f) with a skin friction balance, as a function of flow rates in a subsonic wind tunnel. Onset of fan-induced transition in the tunnel flow provided a unique flow rate for correlating $\Delta\lambda_B$ and C_f values needed for computing effective modulus of rigidity (η_{eff}) of the fiber attached to the metal plate. This value of η_{eff} is expected to remain constant throughout the elastic stress range expected during the Bragg grating aerodynamic tests. It has been used for calculating the value of C_f at various tunnel speeds, on the basis of measured values of Bragg wavelength shifts at those speeds.

14. SUBJECT TERMS
Bragg gratings; Optical fibers; Shear stress; Compressional strain; Temperature effect; Skin friction; Laminar flow; Flow transition; Modulus of rigidity

15. NUMBER OF PAGES
21

16. PRICE CODE
A03

17. SECURITY CLASSIFICATION OF REPORT	18. SECURITY CLASSIFICATION OF THIS PAGE	19. SECURITY CLASSIFICATION OF ABSTRACT	20. LIMITATION OF ABSTRACT
Unclassified	Unclassified	Unclassified	